

RELATION OF KINEMATICS AND CONTACT FORCES IN THREE-BODY SYSTEMS WITH A LIMITED NUMBER OF PARTICLES

Kristin M. de Payrebrune

Institute for Computational Physics in Engineering, TU Kaiserslautern, Germany

Abstract. *In many tribological systems, an intermediate layer of a limited number of abrasive particles exist. Thereby, the resulting wear and friction phenomena are desirable in many manufacturing processes, such as lapping or polishing, whereas in machine elements, they are unwanted due to reducing lifetime or performance.*

For a better understanding of the contact phenomena and the interaction of tribological systems with an intermediate layer of a limited number of particles, fundamental investigations are carried out on a tribometer test rig. For this purpose, two test scenarios are investigated, a) the kinematics and contact forces of single geometrically defined particles such as dodecahedron, icosahedron and hexahedron, and b) the contact forces and surface roughness of a layer of silicon carbide particles of different sizes.

The measured ratio of tangential to normal force can be used as an indicator of the dominating kinematics of the particles and of the generated surface roughness, respectively. The higher the force ratio, the higher the tendency to slide for a given particle type and pairing of particle and counter body.

For one geometrically defined particle the short-time Fourier transform additionally helps to distinguish the state of motion since the excited frequencies during rolling are reduced. For a layer of silicon carbide particles, the velocity and particle size have the strongest influence on the overall motion and the surface roughness produced. Larger particles tend to slide and create more scratches, while smaller particles tend to roll and create indentations in the counter body. Furthermore, for the same particle size, an increase in velocity causes a transition from sliding to rolling, resulting in an increased surface roughness.

Key words: *Three-body contact, Particle kinematics, Contact force analysis, Tangential to normal force ratio, Surface roughness*

Received March 10, 2021 / Accepted April 12, 2021

Corresponding author: Kristin M. de Payrebrune
TU Kaiserslautern, Erwin-Schrödinger-Str. 56, 67663 Kaiserslautern
E-mail: kristin.payrebrune@mv.uni-kl.de

1. INTRODUCTION

Many tribological applications with single or a limited number of particles exist that significantly affect the system. Often these penetrating particles are undesired in technical applications and machine elements, as they reduce the service life or impair the performance. However, in other cases, abrasive particles are used for processing, such as for lapping and polishing, to achieve particularly high surface finishes. In order to obtain the desired surface quality and roughness values, the choice of the appropriate parameters (contact pressure, rotational speed) and their interactions with the particles, as well as the contact phenomena are decisive.

Even though the applications of tribological systems with an intermediate layer of particles are extensive, the area of research often focuses on the dependence of coefficient of friction, wear behavior, or material removal rate on process parameters such as applied force, particle size and sliding speed of the counter body [1-3]. Specific investigations on the surface roughness and interaction between particles and counter body of Hemanth et al. showed an increased roughness at the exit of particles compared to the entry into the contact [4]. Additionally Ahn and Park measured an increased roughness with larger particles, which they attributed to the reduced number of particles in contact [5], whereas Zhang et al. additionally stated that higher wear rate and worn surface features appeared a lower applied loads [6].

Especially for lapping processes detailed analysis of the lapping slurry on the cutting depth are carried out by Belkhir et al. and Wang et al. who stated an increased material removal rate for suspensions that corrode the workpiece surface [7, 8]. Additionally Cozza et al. were able to relate measured coefficients of friction to the kinematics of abrasive particles from different materials. In general a low concentration of abrasive slurry results in a high coefficient of friction and a grooving motion, whereas a high concentration of abrasive slurry let reduce the coefficient of friction and rolling becomes dominant [9]. The adaptation of the particle motion by special lapping plates was also used in the lapping process of Guo et al. to achieve different surfaces roughness [10].

Beside analyses of the overall material removal rate, detailed investigations on single particles help to better understand the local penetration mechanism. Indentation and scratch tests of single particles are therefore standard procedures in order to correlate the particle kinematics with the material failure and the removed material. Thereby, two important findings were established. Firstly, the kinematics of the particles can be directly assigned to the generated surface structures (scratches, indentations), secondly the damage behavior of the material has a significant influence on the final surface [3, 11-13]. Belkhir et al. and Buijs and Korpel-van Houten have observed scratches and cracks starting from the plastic zone below the surface when doing tests on glass samples [7, 14, 15]. They estimated the occurring stresses according to Hertz contact law, so that a prediction of the surface condition was possible. In particular, Heisel and Avroutine developed a model to estimate the kinematics of a particle based on the geometry and contact forces [12]. Vangla et al. introduced two shape parameters that allowed them to characterize granular material and to relate the shape of particles to their tendency to roll or slide [16]. With a more recent molecular dynamics model, Shi et al. investigated the surface indentation of an ellipsoidal particle and observed a transition from rolling to sliding when increasing the normal load [17]. Further studies on elastic particles between

two plates with a boundary element model by Li revealed local stick and slip regions and a subsequent transition from rolling to gliding [18]. In previous works of the author, Bilz and de Payrebrune found comparable dependencies on the motion of a hard, cubical particle. For a constant coefficient of friction, the cube-shaped particle can roll and slide depending on its orientation (contact with edge or corner of a hexahedron), while an increased velocity leads to a detachment of the upper plate and thus to a strongly changed force ratio [19, 20].

Generally, the investigations of single particle contacts have been carried out on defined grits with the aim to relate the particle geometry to the produced surface failure or kinematics. In contrast, lapping investigations focused primarily on the achievable material removal rate and surface quality for different particle properties, lapping slurries and materials of the samples. The results are well established, however, in many tribological systems the geometry of penetrating particles is not defined and measurements of impact parameters are only possible indirect, such as analyzing the overall process forces or the surface roughness after operation.

In our case, we aim to generate a specific microstructure through a customized lapping process by controlling the kinematics of the particles through appropriate process parameters and by using no lapping fluid. Generally, this requires precise knowledge of the interplay between particle kinematics, set parameters and particle properties (shape, size, quantity), which we investigate on the basis of indirectly measurable quantities during the process, such as the forces and the resulting force ratio. Therefore, two fundamental analyses are conducted. Firstly, forces are measured of tribological systems with single particles of different shapes and are linked to the observed particle kinematics. Secondly, this knowledge is used to correlate measured forces of experiments with one layer of particles to their overall kinematics and generated surface.

In the following, the setups and test procedures for individual particles and a layer of particles are explained. Based on these experiments, observations on the behavior of the particles are discussed and an additional relation between surface roughness and particle kinematics introduced, before the main findings are concluded.

2. EXPERIMENTAL INVESTIGATION

The kinematics of individual particles or a layer of abrasive particles directly influences the material removal and the occurring process forces. In order to study these relations, tribometer tests have been carried out.

2.1 General Setup

Two experimental scenarios were developed to investigate local and global interrelations, namely:

- i. Measurement of tangential forces and motion of individual, geometrically defined particles for preset normal forces on different surfaces,
- ii. Measurement of tangential forces of an abrasive layer of silicon carbide particles for preset normal forces and rotational velocities. Subsequently, the achieved surfaces of the samples are tactilely measured and the roughness values correlated with the particle kinematics and force ratio.

Both test scenarios are carried out on a tribometer test rig with three different base plate speeds of 4 rpm, 12 rpm and 22 rpm (75 mm/s, 220 mm/s and 400 mm/s). Via a cantilever arm mounted on one side, a counter plate is pressed onto the particles with a defined normal force. In order to study the kinematics of individual particles, a metal plate is first attached to a 3-axis force dynamometer (type 9119AA1, force range ± 4 kN, Kister) and then to the cantilever arm. For the tests with a layer of abrasive particles a sample holder is mounted on the force sensor to fix steel samples of $30 \times 30 \times 5$ mm. The normal force is set by weights which are attached to the cantilever arm, cf. Fig. 1. In this work, the influence of a liquid on the tribological behavior is explicitly not studied.

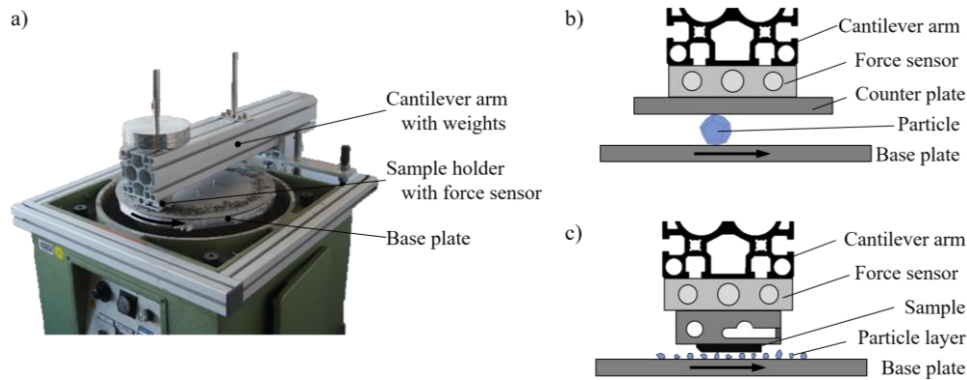


Fig. 1 Tribometer setup for experimental investigations of individual particles and a layer of silicon carbide particles. Photo of the test rig in a), scheme of the setup for one particle in b) and for a layer of particles in c)

2.2 Setup for single particles

The experiments with single acrylonitrile butadiene styrene particles (plastic dice made of ABS) are performed on dodecahedrons, icosahedrons and hexahedrons with an average size of 20 μ m. For both, base plate and counter plate, a smooth steel surface and a sand paper surface with grit size K150 are used, so that four surface combinations are tested. The normal force has been set to 50 N throughout all experiments and the motion behavior is recorded with a high-speed camera (Chronos 1.4, Kron Technologies Inc.) at 4484 fps and the forces are stored accordingly at a sampling rate of 4484 Hz. In addition, the path of the particles is tracked with tracing paper for selected experiments.

Fig. 2a shows exemplary a force profile of the normal and tangential directions, which also reveals the different phases of the experiment. The jump of the normal force at 5 s results when the cantilever arm is set down on the base plate. At about 7 s the motor is switched on and starts rotating with a delay of 3 s. Between the 10th and 13th second the actual experiment takes place, which ends with switching off the engine (at 13 s) and lifting the cantilever arm at 15 s. Depending on the particle motion (rolling or sliding) the duration of the measurement varies. However, during the actual experiment, the particle moves once from its initial left position by angle α to the right end of the plate, cf. Fig. 2b.

The measured tangential force components F_x and F_y represent clearly the angular influence during the actual experiment (10th to 13th second). First, the particle moves in

negative y-direction, which results in a negative force component F_y . During the course of motion, the value becomes positive when the particle starts moving in positive y-direction after intersecting the y-axis. The force component F_x remains positive during the entire test, but varies as a result of the angle between x-axis and tangential force F_t . The applied normal force should actually remain constant, but due to tolerances in the bearing of the cantilever arm a small tilting occurs, which leads to a variance of 1.5 N in F_z . Nevertheless, the force ratio of tangential and normal force

$$\frac{F_t}{F_n} = \frac{\sqrt{F_x^2 + F_y^2}}{F_z} \quad (1)$$

is determined and evaluated for various experiments.

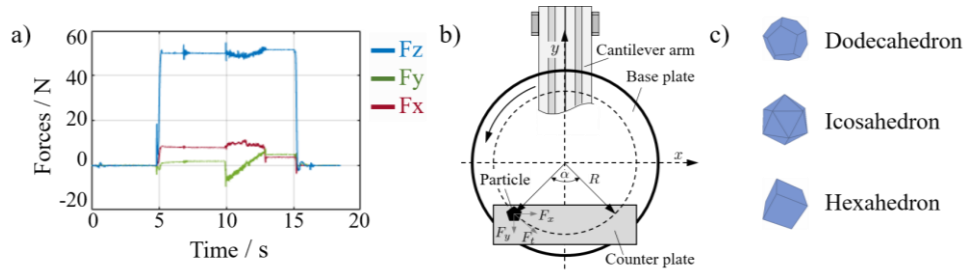


Fig. 2 Representative measurement of process forces with an individual particle in a), scheme of the particle's path in relation to the used coordinate system in b), and shapes of the used particles in c)

2.3 Setup for a layer of particles

The experiments with one particle layer are conducted with particles of silicon carbide of size F12 ($\sim 1765 \mu\text{m}$), F30 ($\sim 625 \mu\text{m}$) and F60 ($\sim 260 \mu\text{m}$), cf. Fig. 3b. The base plate is made of steel, which is renewed after each series of nine tests for a specific particle size. The counter plate is a steel sample of $30 \times 30 \times 5 \text{ mm}$, which is renewed after each experiment. The applied normal forces are set to 40 N, 60 N and 80 N and the duration of experiments are adjusted to the rotational speed of the base plate such that the sliding distance remains the same. During experiments, the forces are recorded at a sampling rate of 1000 Hz in all three directions.

In preparation for each experiment, 50 g of particles are uniformly distributed on the base plate in a ring. During experiments, the clamped steel sample attached to the cantilever arm is first placed on the particle layer and base plate. After the motor has been switched on and started, the test is carried out until a specific sliding distance is reached. In order to detect drifts of the forces, the sample is lifted again at the end of the test, similarly to the test procedure of individual particles. Fig. 3a exemplary shows the force profiles of the normal and tangential directions, and the different phases of the experiment. Because the sample is placed on the point of intersection with the y-axis (cf. Fig. 2b), the force component F_y is almost zero. Nevertheless, the force ratio is calculated from both tangential force components by Eq. (1) and the force ratio is evaluated in

relation to the test settings and the generated surface of the sample. For this purpose, following the experiments, the surfaces of the samples are measured tactilely on a Nanoscan (Hommel-Etamic).

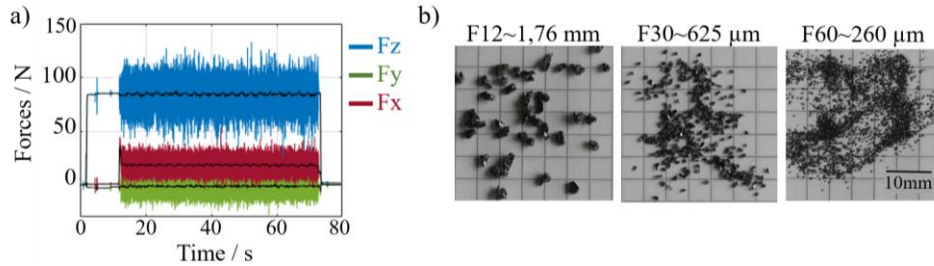


Fig. 3 Representative measurement of process forces for one player of particles in a), and images of investigated silicon carbide particles of sizes F12, F30 and F60 in b)

3. EXPERIMENTAL RESULTS AND DISCUSSION

The aim of these experimental investigations is to correlate the particle kinematics and the generated sample surfaces with process parameters and measured forces in order to better understand tribological systems with a limited number of particles. To this end, the behavior of the individual particles is investigated first. The results obtained are then used to analyze the behavior of a layer of particles in more detail.

3.1 Results for single particles

The experiments with single particles are performed on dodecahedron, icosahedron and hexahedron, whose shape changes from spherical to more and more angular, and for which their motion and related forces are recorded. Besides analyzing the single force components, the ratio of tangential and normal force F_t/F_n and the frequency response are evaluated and are set in relation to the motion and the tracked path of the particles by tracing paper¹.

Figs. 4 to 6 show results of an icosahedron, a dodecahedron and a hexahedron moving on sand paper with grit size K150. Considering the corresponding high-speed videos, the measured forces can be clearly related to the individual motion of the particles. Generally, as soon as the particle starts rolling, the tangential forces drop significantly, whereas during sliding, large amplitudes and vibrations occur.

Depending on whether the particle rolls over a corner or over an edge, the force fluctuation varies in strength, compare [19]. According to high-speed videos of the dodecahedron (cf. Fig. 4), the particle rolls over an edge at motion {1, 4, 7, 10, 13, 15}, which can also be obtained from the lower decrease in the force ratio F_t/F_n , or a smaller

¹Only for the special measurements for tracking the particle trace was the test rig modified so that the cantilever arm points in the x-direction instead of the y-direction (cf. Fig. 2a). This modification has the effect of increasing the normal force when the particle moves in the positive x-direction since the lever arm between the pivot point of the cantilever and the point of contact is reduced. All measurements for the analysis of the force ratio are carried out with the original setup

increase in F_x , respectively. The force component F_y varies similar to F_x , except that the sign depends on whether the particle rolls in positive or negative y-direction, cf. Figs. 4a and c.

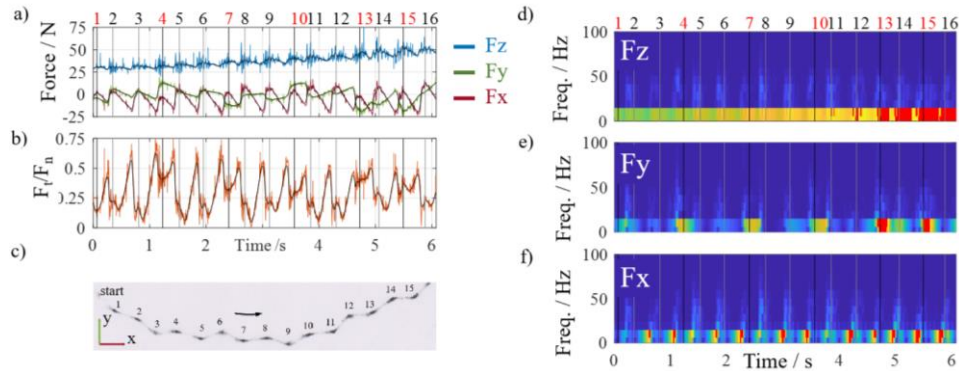


Fig. 4 Force measurements with displayed components F_x , F_y and F_z in a), calculated force ratio F_t/F_n in b), and tracked path with tracing paper in c) for experiments with an individual **dodecahedron** and 4 rpm. Short-time Fourier transform of the force components are shown in d)-f). Numbers indicate the beginning of rolling.

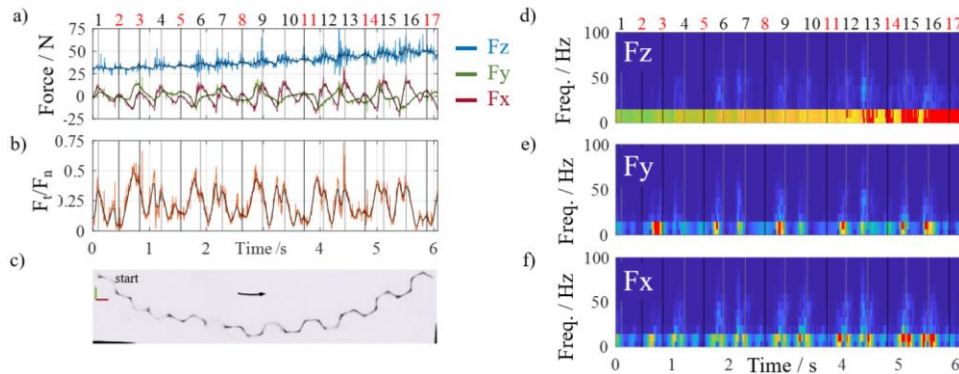


Fig. 5 Force measurements with displayed components F_x , F_y and F_z in a), calculated force ratio F_t/F_n in b), and tracked path with tracing paper in c) for experiments with an individual **icosahedron** and 4 rpm. Short-time Fourier transform of the force components are shown in d)-f). Numbers indicate the beginning of rolling.

For the icosahedron, similar force progressions have been observed with regard to rolling over an edge or a corner, cf. Fig. 5. However, when the counter plate has contact with a flat surface of the icosahedron, a short sliding motion occurs before the next rotation over a corner or edge starts, which results in normal force fluctuations. Compared to the dodecahedron, the amplitude increase is stronger for the icosahedron, which indicates a higher resistance to rolling.

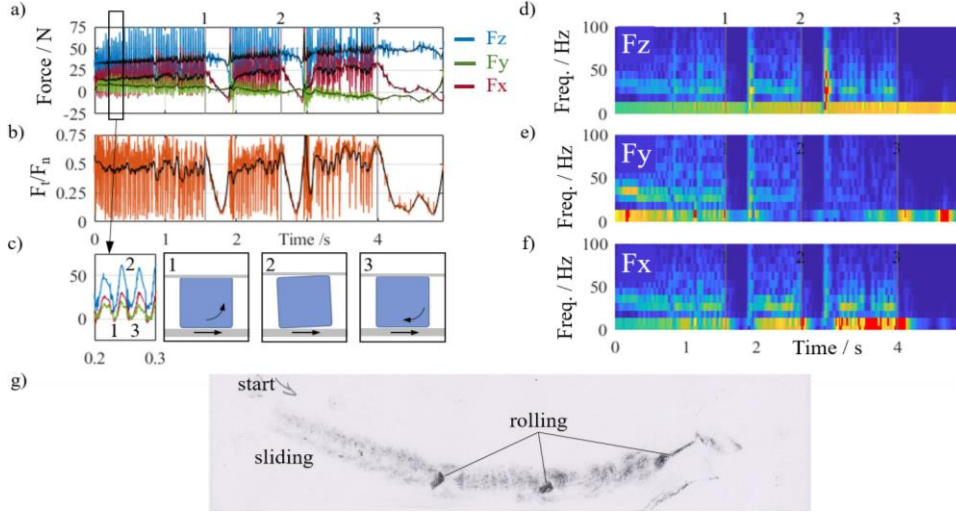


Fig. 6 Force measurements with displayed components F_x , F_y and F_z in a), calculated force ratio F_t/F_n in b) and zoomed forces during sliding with the corresponding motion in c) of experiments with an individual **hexahedron** and 4 rpm. Short-time Fourier transform of the force components are shown in d)-f), and tracked path with tracing paper in g). Numbers indicate the beginning of rolling.

In comparison to the icosahedron and dodecahedron, the hexahedron is very angular and has a very high resistance to rolling, which results in large vibrations of the measured forces in Fig. 6. By help of the high-speed videos, the local oscillating forces can be related to a repeatedly tilting of the hexahedron (peak at 2 in Fig. 6c), but instead of proceeding rolling, the hexahedron flips back on its flat face (drop at 3).

Generally, as soon as the tangential force is large enough to start rolling, the tangential forces decreases significantly and the force ratio becomes $F_t/F_n|_{\min}=0.04$, regardless of the shape of the particle. Hence, both values, the tangential force component F_x and the force ratio F_t/F_n are valid indicators to distinguish different motions of the individual particles.

Beside the force analyses, the frequency response of each force component is additionally evaluated. Therefore, a short-time Fourier transform (STFT) is performed of 500 measured values each of every 0.55 s, which results in a frequency resolution of 8.9 Hz. The STFT of the three particle shapes are displayed as color maps in Figs. 4d-f to 6d-f. As soon as the particle starts rolling the STFTs of F_x show a significant frequency decrease at low values (0-10 Hz), accompanied by decreased amplitudes of F_y when the particle rolls over an edge and radial motion occurs. Furthermore, at higher frequencies between 20 Hz and 80 Hz, the STFT of F_z shows a strong excitation during sliding and a drastic decrease during rolling (especially visible for the hexahedron cf. Fig. 6). Consequently, the STFT of the measured forces also helps to distinguish the different states of motion of the individual particles.

In order to transfer these findings to a particle layer in which only statements about the overall behavior of all particles can be made, the observed kinematics of the individual particles are correlated to averaged values of the force ratio F_t/F_n , as displayed in Fig. 7a.

In here, all experiments are grouped in red where either the rotating plate and/or the counter plate is a smooth steel surfaces and the corresponding high-speed videos show a pure sliding movement of the particle. The force ratio of $F_t/F_n \approx 0.2$ is almost constant with low variances, compare also with Fig. 7b. In contrast, when both plates are covered with sand paper, the average force ratio depends on the rolling ability of the particle, as the results in Fig. 7a show in blue. The more frequently a particle rolls and the less the contact duration of upper plate with a flat surface of the particle is, that results in increased force amplitudes of F_n , the lower the force ratio becomes.

Comparing the force ratios for overall rolling of a dodecahedron and an icosahedron, this is particularly evident when comparing the results in Fig. 4, Fig. 5. When the particles roll to one of their flat sides a short sliding follows. As a result, the force ratio increases to values in the same range as those of the sliding hexahedron (cf. Fig. 7c) and the normal forces show increased amplitudes. Related to the number of surfaces of the particle geometry, the different contact situations (contact with flat surface, edge or corner) changes more rapidly for the icosahedron with 20 surfaces than for the dodecahedron with 12 surfaces. In addition, due to its more spherical shape compared to the icosahedron, the dodecahedron can more easily roll, which reduces the time intervals with strong force fluctuations. Consequently, the influence of the intermediate sliding dominates for the icosahedron and leads to a higher mean force ratio than for the dodecahedron.

Due to the angular shape of the hexahedron, it slides over long periods of time, which results in a much higher overall force ratio on sand paper with $F_t/F_n = 0.52$ than for the other particle geometries. However, when determining the force ratios of pure rolling and pure sliding, the force ratios show a clear distinction between both motions, as indicated in Fig. 7a in green. Consequently, the force ratio for rolling is not influenced by sliding periods, which results in a lower value compared to the other geometries and the force ratio for sliding with $F_t/F_n = 0.58$ exceeds slightly the mean force ratio. So by knowing the lower and upper boundary for rolling and sliding, the value of the force ratio indicates the ratio of both states of motion.

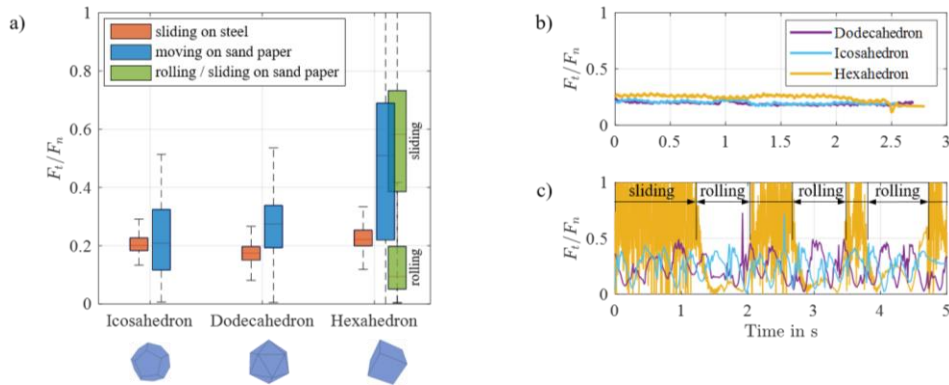


Fig. 7 Force ratio F_t/F_n of dodecahedrons, icosahedrons and hexahedrons. Mean force ratio on different surfaces with shown median value, first quartile, third quartile and whiskers based on the interquartile range in a). Force ratio as a function of time during sliding on steel in b) and force ratio during rolling, or sliding and rolling in the case of a hexahedron, respectively on sand paper in c).

Table 1 Average values and standard deviation σ of force components with an applied normal force of 50 N and rotational speed of 4 rpm, and tracked path according to the geometry of the individual particle when both plates are covered with sand paper



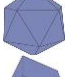

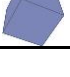
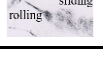
Geometry		F_t	F_n	$F_t/F_n \pm \sigma$	Trace
Dodecahedron		11.27 N	50.15 N	0.22 ± 0.12	
Icosahedron		14.169 N	49.20 N	0.28 ± 0.08	
Hexahedron		23.93 N	48.97 N	0.52 ± 0.4	

Table 1 lists the average values of the force components the ratio of F_t/F_n and its standard deviation when both plates are covered with sand paper of grit size K150. Generally, we can state that the smaller the average force ratio is, the more frequent the particle rolls, and the results for individual, geometrically defined particles can be summarized as follows:

- The tangential force needs to overcome the resistance against rolling. If the tangential force is too small, the particles slide on smooth surfaces and chatter on rough surfaces.
- The force progression and the short-time Fourier transform can be used to distinguish between rolling and sliding of the particle. When the particle rolls, the force ratio significantly drops and the amplitudes in the frequency domain decreases.
- Also the mean value of the force ratio can be used to distinguish between different states of motion. When knowing the force ratios of pure rolling and pure sliding, the force ratio indicates the ratio between both states of motion.

3.2 Results for a layer of particles

The analysis of one layer of silicon carbide particles is analogous to the analysis of individual particles. During the experiments, the normal and tangential force components are recorded, however, the mean force ratio is calculated from the filtered values, which is done by using a first order Butterworth filter with a cut-off frequency of 100 Hz. In addition, roughness parameters obtained from tactile surface measurements of the steel samples are analyzed.

Fig. 8 shows the average force ratio F_t/F_n in terms of all three analyzed parameters: particle size (F12, F30, F60), rotational speed of base plate (4 rpm, 12 rpm, 22 rpm), and applied normal force ($F = 40$ N, $F = 60$ N, $F = 80$ N). Here, no dependence on the normal force is noticeable. However, the force ratio depends and partly on the speed of the base plate and strongly on the particle size, whereby the absolute values of the force ratio become smaller with decreasing size. The strongest influence on the rotational speed show particles of size F30 with a force ratio that decreases from $F_t/F_n = 0.27$ to $F_t/F_n = 0.20$, while the other particle sizes lead to more constant values.

According to the results of individual particles a high force ratio indicates sliding and chattering. Applied to the measurements of one particle layer, this means that the particles

of size F12 slide more frequently than the smaller particles. Images of the sample surfaces confirm this assumption. Fig. 9 shows the generated surfaces and tactically measured surface profiles for a normal force of $F_z = 40$ N and various particle sizes and speeds. In accordance to the large force ratio of particles F12, all samples show numerous scratches over the entire surface due to a dominant sliding motion.

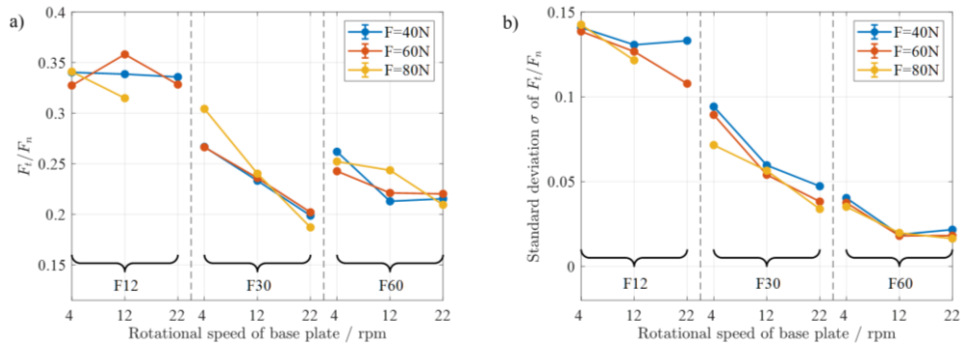


Fig. 8 Mean values of force ratio F_t/F_n in a) and corresponding standard deviation in b) of measurements with one layer of particles and for different parameters.

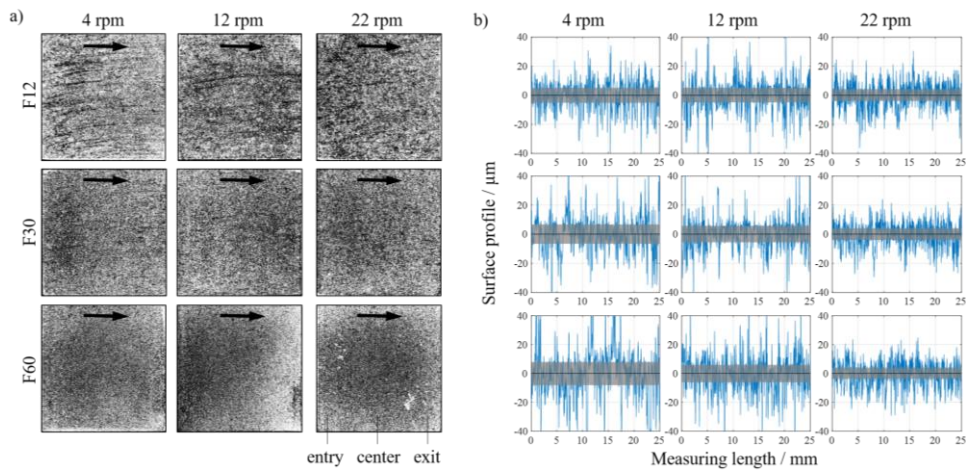


Fig. 9 Black and white surface images of steel samples generated with different silicon carbide particles, rotational speeds and with an applied normal force $F_z = 40$ N. The arrow indicates the direction of particle motion with the upper side pointing outwards in a). Tactile measured surface profiles with standard deviation of profiles at the entry, center and exit at each sample in b).

Transferring the findings of individual particles to the measured force ratio for a particle layer with size F30, the tendency to roll should increase with rotational speed of the base plate. The corresponding surface images confirm this, as large scratches are only found at low speeds (cf. Fig 9a) and with higher velocity the scratches shorten. Hence,

these particles perform a transition from sliding to primarily rolling as a function of the rotational speed. In contrast, of the smallest particles of size F60, the mean force ratio and standard deviation, as well as the surface images indicate a predominant rolling motion. Accordingly, the surface structure produced by a layer of silicon carbide particles correlates with the state of motion predicted by the force ratio and can also be distinguished in the roughness measures.

The surface profiles are measured orthogonal to the direction of particle motion at the entrance, center and exit of particles at each sample (cf. Fig. 9a), with the standard deviation of the three profiles shown as a gray ribbon in Fig. 9b. The corresponding arithmetical mean deviation R_a and the core roughness R_k are additionally calculated and averaged over six standard measuring lengths of 12.5 mm at each position, which are placed within the surface profile. As evident from Fig. 10, the arithmetic mean deviation R_a and the core roughness R_k increase with velocity and normal force. In conjunction with the measured reduction of the force ratio at higher speeds for particle size F30, it becomes apparent that higher roughness values are related to an increased rolling motion.

Even if the experiments with individual particles did not result in any material removal, statements about the contact conditions can be made on the basis of the recorded traces. Especially evident at the trace of a hexahedron cf. Fig. 6g, sliding causes a wide and brighter trace than rolling, for which dark concentrated dots can be seen when a corner or edge is in contact. These higher contact stresses during rolling results in deeper indents, as already observed from [14, 15]. Transferred to the particle layer, for a fixed particle size deeper indentations and a higher roughness result during rolling than sliding, as visible for F30. Furthermore, the indents become deeper with particle size and normal force, and the roughness increases, as previously observed [5].

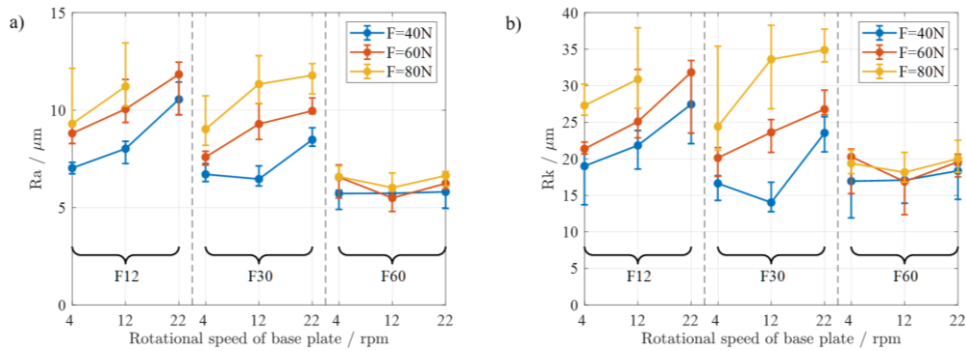


Fig. 10 Arithmetical mean deviation R_a in a) and core roughness R_k in b) of steel sample surfaces generated by tribometer tests with a layer of silicon carbide particles as a function of particle size, base plate speed, and applied normal force. Shown are the median values with first quartile and third quartile as error bars calculated from surface profiles at all locations on one sample.

According to the good correlation of observations on individual particles and one layer of particles, the following statements on the motion behavior can be made:

- a) The average force ratio F_t/F_n and its standard deviation σ are valid parameters to distinguish different motion tendencies of the particle layer. Thereby, the results of a particle layer matches the observations of individual particles.
- b) In general, the states of motion depend less on the applied forces than on the speed and particle size.
- c) There is a size dependence with regard to the states of motion and the influence of process parameters. For the parameters investigated, the largest particles (F12) show predominantly sliding, the smallest particles (F60) predominantly rolling, and the medium-sized particles (F30) a transition from sliding to rolling.
- d) According to the state of motion, rolling results in higher localized stresses and consequently in deep indents and a high roughness, whereas sliding results in scratches with a lower roughness. Additionally the roughness values increases with normal force and particle size.

4. CONCLUSION

The movement of individual, non-abrasive particles and a layer of abrasive silicon carbide particles was investigated by tribometer tests. The tests on single particles were performed with three geometric shapes (dodecahedron, icosahedron, hexahedron) on smooth steel surfaces and on rough sand paper with grit size K150. During experiments with one layer of particles, the particle size, the speed of the base plate and the normal force have been varied.

The analyses show that the average force ratio F_t/F_n of the tangential and normal force components and their standard deviation σ are valid indicators to distinguish different states of motion for both test cases. For the same surface pairing and particle shape, a reduction in the force ratio means an increase in rolling, which is associated with a reduction of the standard deviation due to a more uniform motion. If the force ratios for pure rolling and sliding are known, the average force ratio can be used to determine the proportion of sliding and rolling. In both test cases, the tendencies of the force ratio and the standard deviation are similar, so that observations about the state of motion of individual particles can be transferred to systems with an intermediate layer of particles.

Based on the recorded trace of individual particles, contact with a corner or edge results in darker imprints than when the flat side of the particle is in contact during sliding. Consequently, rolling results in deeper indentations, which leads to a higher roughness. Additionally, the roughness increases with a larger particle size and higher applied loads. However, due to the complex relationships between particle size, motion type and roughness value, reference measurements must be carried out for each particle type and material pairing.

In general, the correlation found between the state of motion and the mean force ratio, its standard deviation, and roughness measures can be used as an indicator of motion, and to change the system behavior in a desired way. Both findings of the force analysis and the roughness values additionally help to characterize tribological systems and increase the understanding about the complex phenomena in the contact.

Acknowledgement: *The work is funded by the Deutsche Forschungsgemeinschaft (DFG, German Research Foundation) – Project-ID 172116086 – SFB 926.*

REFERENCES

1. Stachowiak, G.B., Stachowiak, G.W., 2001, *The effects of particle characteristics on three-body abrasive wear*, *Wear*, 249(3-4), pp. 201-207.
2. Agbaraji, C., Raman, S., 2009, *Basic observations in the flat lapping of aluminum and steels using standard abrasives*, *The International Journal of Advanced Manufacturing Technology*, 44(3), pp. 293-305.
3. Cho, B.-J., Kim, H.-M., Manivannan, R., Moon, D.-J., Park, J.-G., 2013, *On the mechanism of material removal by fixed abrasive lapping of various glass substrates*, *Wear* 302(1-2), pp. 1334-1339.
4. Hemanth, G., Suresha, B., Hemanth, R., 2019, *The effect of hexagonal boron nitride on wear resistance under two and three-body abrasion modes of polyetherketone composites*, *Surface Topography: Metrology and Properties*, 7(4), 045019.
5. Ahn, Y., Park, S.-S., 1997, *Surface roughness and material removal rate of lapping process on ceramics*, *KSME International Journal*, 11, 494.
6. Zheng, B., Li, W., Tu, X., Song, S., Huang, W., 2019, *Effect of ZTA ceramic particles strengthened high chromium white cast iron on three-body abrasion behavior*, *Materials Research Express*, 6(11), 116581.
7. Belkhir, N., Bouzid, D., Herold, V., 2009, *Surface behavior during abrasive grain action in the glass lapping process*, *Applied Surface Science* 255(18), pp. 7951-7958.
8. Wang, Z.K., Wang, Z.K., Zhu, Y.W., Su, J.X., 2015, *Effect of lapping slurry on critical cutting depth of spinel*, *Applied Surface Science* 347, pp. 849-855.
9. Cozza, R.C., Wilcken, J.T.D.S.L., Schön, C.G., 2018, *Influence of abrasive wear modes on the coefficient of friction of thin films*, *Tecnologia em Metalurgia, Materiais e Mineração*, 15(4), pp. 504-509.
10. Guo, L., Zhang, X., Chen, S., Hui, J., 2019, *An experimental study on the precision abrasive machining process of hard and brittle materials with ultraviolet-resin bond diamond abrasive tools*, *Materials*, 12(1), 125.
11. Belkhir, N., Bouzid, D., Herold, V., 2007, *Correlation between the surface quality and the abrasive grains wear in optical glass lapping*, *Tribology International* 40(3), pp. 498-502.
12. Heisel, U., Avrutine, J., 2001, *Process analysis for the evaluation of the surface formation and removal rate in lapping*, *CIRP Annals – Manufacturing Technology* 50(1), pp. 229-232.
13. Li, C., Cai, G., 2006, *Material removal mechanisms analysis in the finishing machining of engineering ceramics*, *International Conference on Programming Languages for Manufacturing*, Springer, Boston, MA, pp. 729-734.
14. Buijs, M., Korpel-van Houten, K., 1993, *A model for lapping of glass*, *Journal of Materials Science* 28(11), pp. 3014-3020.
15. Lawn, B.R., Evans, A.G., Marshall, D.B., 1980, *Elastic/plastic indentation damage in ceramics: The median/radial crack system*, *Journal of the American Ceramic Society* 63(9-10), pp. 574-581.
16. Vangla, P., Roy, N., Gali, M.L., 2018, *Image based shape characterization of granular materials and its effect on kinematics of particle motion*, *Granular Matter*, 20(1), pp. 1-19.
17. Shi, J., Chen, J., Wei, X., Fang, L., Sun, K., Sun, J., Han, J., 2017, *Influence of normal load on the three-body abrasion behaviour of monocrySTALLINE silicon with ellipsoidal particle*, *RSC advances*, 7(49), pp. 30929-30940.
18. Li, Q., 2020, *Simulation of a single third-body particle in frictional contact*, *Facta Universitatis-Series Mechanical Engineering*, 18(4), pp. 537-544.
19. Bilz, R., de Payrebrune, K.M., 2019, *Analytical investigation of the motion of lapping particles*, *PAMM*, 19(1), e201900076.
20. Bilz, R., de Payrebrune, K.M., 2021, *Investigation of the influence of velocity in a tribological three-body system containing a single layer of rolling hard particles from a mechanical point of view*, *Tribology International*, 159, 106948.